ACS NANO
Cite This: ACS Nano XXXX, XXX, XXX−XXX
www.acsnano.org

ARTICLE

Small-Band-Offset Perovskite Shells Increase Auger Lifetime in Quantum Dot Solids

Rafael Quintero-Bermudez,[†] Randy P. Sabatini,[†] Marc Lejay, Oleksandr Voznyy,* and Edward H. Sargent*

Department of Electrical and Computer Engineering, University of Toronto, 10 King's College Road, Toronto, Ontario M5S 3G4, Canada

Supporting Information

ABSTRACT: **Colloidal quantum dots (CQDs) enable low-cost, high-performance optoelectronic devices including photovoltaics, photodetectors, LEDs, and lasers. Continuous-wave lasing in the near-infrared remains to be realized based on such materials, yet a solution-processed NIR laser would be of use in communications and interconnects. In infrared quantum dots, long-lived gain is hampered by a high rate of Auger recombination. Here, we report the use of perovskite shells, grown on cores of IR-emitting PbS CQDs, and we thus reduce the rate of Auger recombination by up to 1 order of magnitude. We employ ultrafast transient absorption spectroscopy to isolate distinct Auger recombination phenomena and study the effect of bandstructure and passivation on Auger recombination. We corroborate the experimental findings with model-based investigations of Auger recombination in various CQD core−shell structures. We explain how the band alignment provided by perovskite shells comes close to the optimal required to suppress the Auger rate. These results provide a step along the path toward solution-processed near-infrared lasers.**

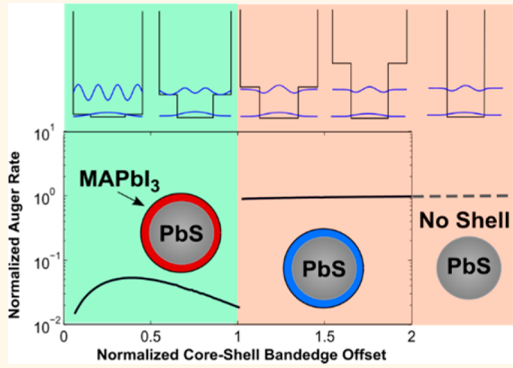

KEYWORDS: *quantum dots, Auger recombination, perovskites, transient absorption spectroscopy, infrared light emission*

Colloidal quantum dots (CQD) synthesis, photophysics, and applications have seen substantial advances in recent years.[1−5] CQDs combine high photoluminescence quantum yields, narrow emission line widths, size-tunable emission, and solution-processability for optoelectronic devices.[6,7] Recently, continuous-wave lasing was shown at visible wavelengths using CQDs.[5] Near-infrared counterparts, of interest in communications, computing,[8] and biology,[9] remain less advanced along the path to CW lasing.

IV−VI semiconductor CQDs such as PbS and PbSe are among the most extensively studied for NIR applications.[6] Their size-tunable synthesis and narrow polydispersity are now well mastered.[10−12] Lead chalcogenide CQDs have been demonstrated to exhibit optical gain,[13,14] ASE,[13,15] and lasing when excited using picosecond pulses;[16] however, CW lasing has so far been elusive. One major limitation, their short gain lifetime (τ_{gain} < 40 ps at room temperature)[16] arises from efficient nonradiative Auger recombination in narrow-gap semiconductor CQDs.[17] Furthermore, lead chalcogenide CQDs require at least four excitons to achieve population inversion, a regime in which Auger recombination is strongly enhanced.

Auger recombination can occur *via* three possible pathways: (1) intradot biexciton Auger recombination, (2) trap-assisted Auger recombination, and (3) diffusion-assisted Auger recombination (Figure 1). Intradot biexciton Auger recombination occurs when two excitons form within a single quantum dot; one exciton then recombines, transferring energy nonradiatively to a remaining charge carrier. The transferred energy will in turn be lost rapidly *via* thermal relaxation of the hot charge carrier. In trap-assisted Auger recombination, one charge carrier in an exciton fills a trap, and energy is subsequently transferred to another band-edge charge carrier. Generally, trap-assisted Auger has been found to exhibit faster Auger recombination rates than those exhibited by a typical biexciton, rendering trap-assisted Auger recombination particularly detrimental to photoluminescence quantum yield (PLQY).[18] In diffusion-assisted Auger recombination, the concentration of charge carriers in a quantum dot is increased by means of diffusion. The larger charge carrier concentrations lead to a higher probability of nonradiative Auger recombination. The latter mechanism increases with charge-carrier mobility.[19−21]

Strategies to reduce these effects have included passivating ligands,[22] low-trap quantum dot syntheses,[10,11] and core−shell structures.[23] Each has improved PLQY significantly by

Received: September 6, 2017
Accepted: December 11, 2017
Published: December 11, 2017

© XXXX American Chemical Society

DOI: 10.1021/acsnano.7b06363
ACS Nano XXXX, XXX, XXX−XXX

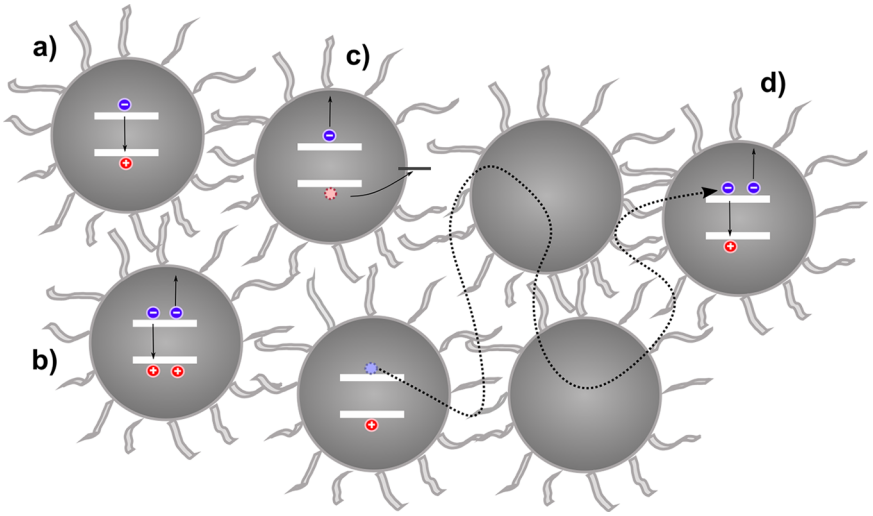

Figure 1. Auger recombination processes. (a) Radiative recombination (b) Traditional intradot biexciton Auger recombination. (c) Trap-assisted Auger recombination, where a carrier interacts with a trap state. (d) Diffusion-assisted Auger recombination.

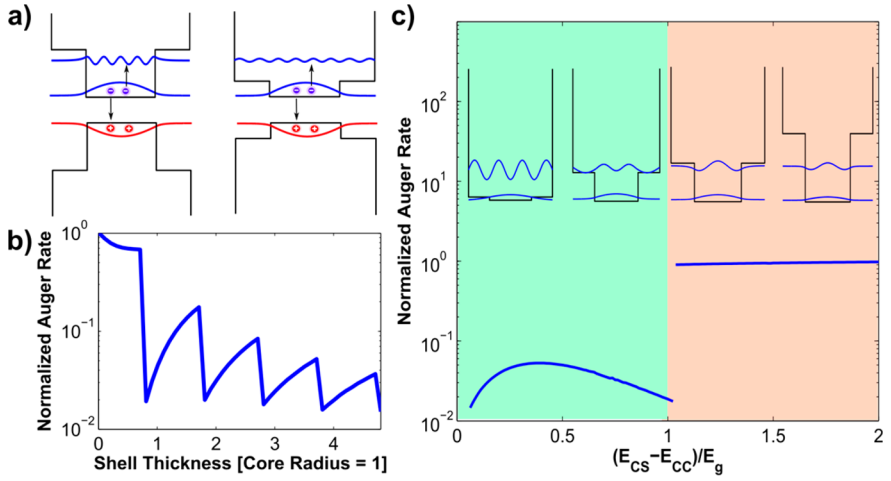

Figure 2. Modeling Auger recombination in CQDs. (a) Charge carrier wave functions in systems where Auger couples to confined continuum states (left) and systems where Auger couples to delocalized continuum states (right). (b) Change in Auger recombination rates as a function of shell thickness. (c) Change in Auger recombination rates as a function of core−shell conduction band offset; E_{CS}, E_{CC}, and E_g represent the shell band edge, core band edge and core bandgap, respectively. Three regimes are identified: DD (delocalized−delocalized): delocalized band-edge state couples to delocalized high-order mode (left green); LD (localized−delocalized) localized band-edge state couples to delocalized high-order mode (right green); and LL (localized−localized): localized band-edge state couples to localized high-order mode (red).

mitigating trap-assisted pathways. These strategies have enabled advances in CQD photovoltaics[7] and photodetectors,[24] although the impact of such strategies on intradot Auger recombination in lead chalcogenide CQDs has not been demonstrated.

The suppression of Auger recombination has been demonstrated in allied CQD systems (CdSe[25,26] and InAs[27]) through the use of judiciously optimized core−shell structures. We posited that, with an appropriate shell, we could inhibit intradot Auger recombination in PbS NIR quantum dots. CdS shells have been grown on PbS; however, synthetic challenges arise in growing thick shells larger than one to two monolayers.[23]

Recently, the development of perovskite shelling has enabled the growth of thicker shells on PbS CQDs:[28−30] 1 nm thick perovskite shells have recently been documented.[28] These new core−shell structures have facilitated the development of efficient detectors,[31] solar cells,[28] and LEDs.[32]

Herein we find, with the aid of ultrafast transient absorption spectroscopy (TAS), that $MAPbI_3$ perovskite shelling decreases the rate of Auger recombination by over 1 order of magnitude. We distinguish, and quantify separately, the effects of passivation and wave function delocalization associated with bandstructure engineering. We distinguish these effects by comparing perovskite shelling to a number of different approaches to CQD passivation. These results provide the foundation for further work on lead chalcogenides in the pursuit of NIR CW lasing.

RESULTS AND DISCUSSION

Theoretical Model. We first sought to quantify the effect of the shell's properties on the intradot biexciton Auger

DOI: 10.1021/acsnano.7b06363
ACS Nano XXXX, XXX, XXX−XXX

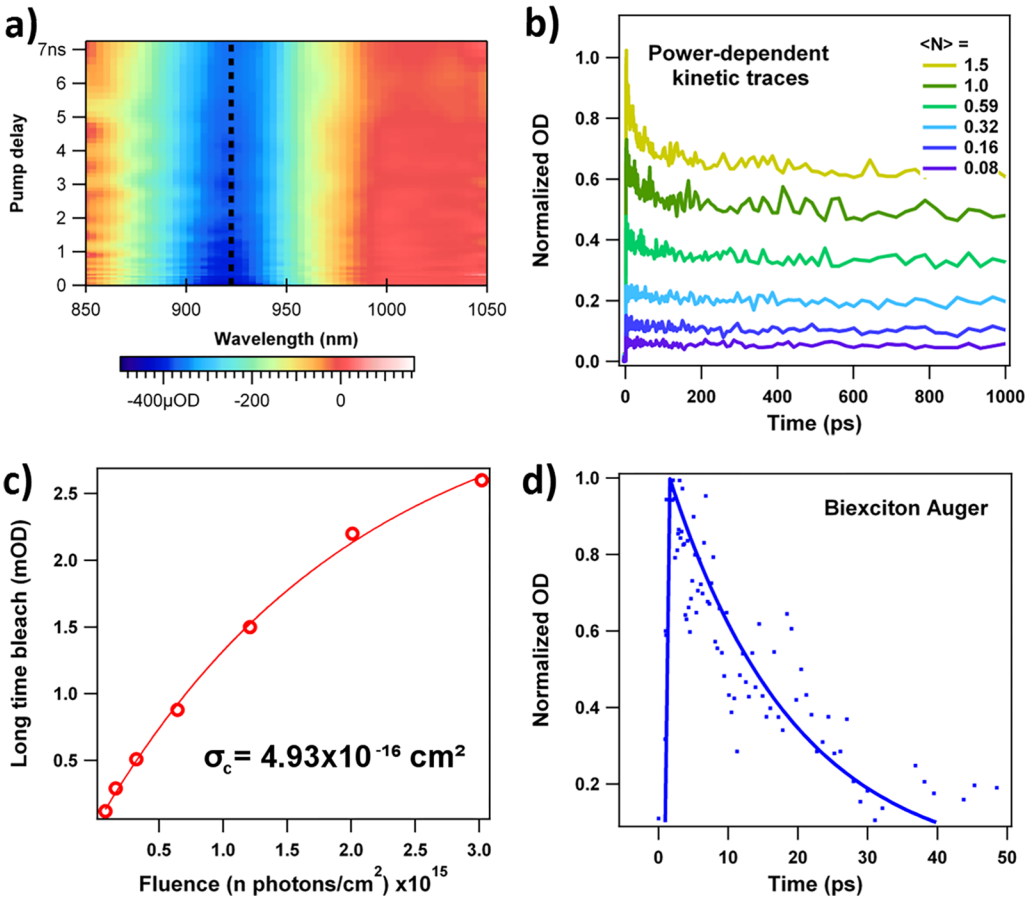

Figure 3. Auger recombination rate analysis. (a) Contour plot of CQD-OLA, showing spectral changes as a function of time. (b) Power dependent kinetic traces at the exciton bleach. (c) TA signal at long times, after Auger recombination, as a function of pump fluence. Fitting this curve allows calculation of excitons per dot. (d) Isolated decay curve of biexciton Auger recombination.

recombination in PbS CQD core−shell systems. The Auger rate can be calculated using Fermi's golden rule[33]

$$\frac{1}{\tau_A} = \frac{4\pi^2}{h}|M_{if}|^2 \frac{1}{\Gamma_f} \quad (1)$$

where M_{if} is the electronic matrix transition element of the Coulomb interaction coupling the initial (i) and final (f) excitonic configurations, and Γ_f is the total dephasing rate of the final higher order carrier; the latter accounts for a mismatch between these discrete state transitions and can be understood as a broadening term. In eq 1, the Auger recombination rate is controlled by the transition element M_{if}, which can be determined using one-dimensional wave functions by

$$M_{if} = \langle \Psi_i | V(x_1 - x_2) | \Psi_f \rangle \quad (2)$$

$$= \int \varphi^*_{cbe}(x_1)\varphi^*_{cbe}(x_2)V(x_1 - x_2)\varphi_{vbe}(x_1)\varphi_{cbc}(x_2)\, dx_1\, dx_2 \quad (3)$$

where the potential, V, is the Coulomb repulsion between charge carriers, $V(x) = e^2/\kappa|x|$, and φ_{cbe}, φ_{vbe}, and φ_{cbc} represent the conduction band edge, valence band edge, and conduction band continuum wave functions, respectively. Details of computations are provided in the Supporting Information.

We validate the model by calculating the dependence of Auger recombination on shell thickness (Figure 2b). We find that the rate of Auger recombination is strongly inhibited as the thickness of the shell is increased, in agreement with previous work.[25,33] As the shell thickness is increased, the contrast is also increased between the localized band-edge carrier and the delocalized Auger-excited continuum mode. This contrast is directly manifested as a reduction in the Coulomb integral determining the matrix element in eq 2. In addition to the general trend, however, the matrix element exhibits an oscillatory behavior as a function of shell thickness, which has been reported previously in theoretical work that employed a Kane model formalism.[33,34]

To explore the optimal core−shell band structure for suppressed Auger, we studied the effect of varying core−shell band edge offsets. We identified three distinct regimes of influence of confinement on Auger rates as a function of the amplitude of the conduction/valence band-edge offset (Figure 2c).

The first, for the case of a small conduction/valence band-edge offset, we term the delocalized/delocalized regime: the lowest lying state extends substantially over the entire extent of the core/shell dot, as does the higher lying continuum mode. As a result, the matrix element, M_{if}, is appreciably reduced relative to the unconfined case. This stems from a delocalization of the single-lobed excitonic mode and a concurrent delocalization of the multinoded continuum mode reducing the modal overlap. As the offset is increased, we enter the localized/delocalized regime, wherein the lowest lying state is now localized to the shell, whereas the higher lying state remains unconfined. In this case, the matrix element remains small due to minimal modal overlap. In the third, highest offset regime, both the initial and final states are localized. This

DOI: 10.1021/acsnano.7b06363
ACS Nano XXXX, XXX, XXX−XXX

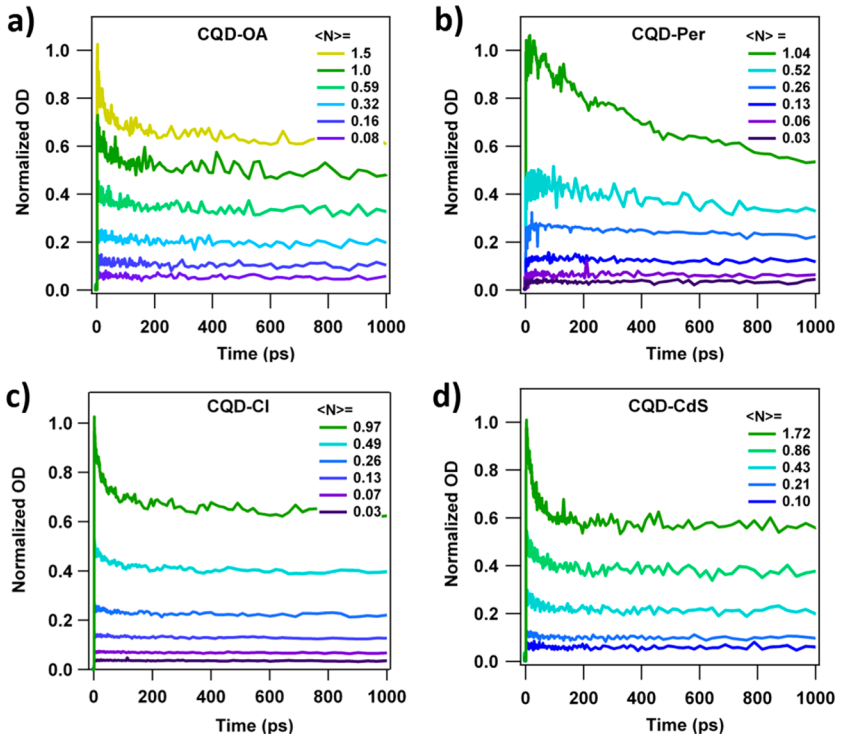

Figure 4. Power dependent Auger recombination. Power dependent kinetic traces at the exciton bleach for (a) CQDs-OLA, (b) CQD-Per, (c) CQD-Cl, and (d) CQD-CdS. Auger lifetime of CQD-Per is much longer than the other samples.

provides a maximum overlap and the highest Auger rate observed herein.

We find that small-offset shells are best at keeping in the delocalized/delocalized regime and minimizing Auger compared to the higher offset cases. Interestingly, the PbS-$MAPbI_3$ perovskite system has a small conduction/valence band offset with respect to PbS,[35] and we thus identified it to be promising to reduce Auger recombination in PbS CQDs.

Auger Recombination in Perovskite-Shelled PbS. We next sought to investigate experimentally the effect of perovskite shelling on Auger recombination. The TAS data collected for a CQD film exhibit a single ground-state bleach (Figure 3a). Due to thermal relaxation, this bleach red-shifts over time to the band edge, and it is at this band-edge wavelength that we perform the analysis that follows.

TAS measurements are collected at various pump fluences in order to ascertain the dependence of the band-edge bleach on the pump power (Figure 3b). The presence of intradot Auger recombination is signaled by the emergence of a second, faster decay rate. We plot the long-time bleach (*i.e.*, ~8 ns) as a function of pump fluence and fit to $B = B_0(1 - \exp(-\langle N_p\sigma_c\rangle))$. By applying this simple model in which the only assumption is of Poissonian statistics,[36] we acquire σ_c, the absorption cross-section per dot (Figure 3c). This value is used to determine the average number of excitons per dot produced by a given pump fluence, $\langle N\rangle$ (Figure 3b).

At low pump fluences ($\langle N\rangle \ll 1$), multiphoton absorption is negligible, and we observe only single exciton recombination. At intermediate pump fluences ($\langle N\rangle \approx 1$), shorter-lived biexciton intradot Auger recombination can be discerned. At higher pump fluences, Auger recombination dominates. We sought to separate out the various multiphoton Auger processes: to do this we employed multiple exponential fittings at each pump fluence, allowing us to extract the biexciton intradot Auger lifetime (Figure 3d).

We carried out this Auger recombination lifetime analysis both on oleic acid passivated 950 nm PbS CQDs (CQD-OA, Figure 4a) and also on perovskite-shelled 950 nm PbS CQDs (CQD-Per, Figure 4b). The 950 nm CQD-OA film exhibited an Auger lifetime of 17 ± 3 ps, and this agrees well with previously reported values.[37,38] It is important to distinguish the effect of diffusion-assisted Auger (Figure 1d) on the TAS traces to avoid misinterpretation. Diffusion-assisted Auger becomes appreciable in highly conductive films, such as the CQD-Per film, which enable charge carrier transfer between dots thus promoting Auger recombination. Diffusion-assisted Auger does not pose an obstacle to achieving gain in these materials, in contrast with intradot Auger, since the gain lifetime is limited by the fastest Auger recombination process, and intradot Auger recombination is faster than diffusion-assisted Auger in each sample studied herein. After we account for diffusion-assisted Auger in CQD-Per films (SI), the intradot Auger lifetime is found to exhibit an improvement of over one order-of-magnitude when perovskite shelling is employed on 950 nm CQDs (Table 1). A summary of these decay processes, their lifetime, and their respective contributions to the ultrafast transient is provided in Table S7.

We then investigated the origins of this dramatic improvement. Specifically, we hypothesized that it could stem either from the core–shell band structure discussed above, directly impacting the M_{if} matrix element, or alternatively, differences in the degree of surface passivation could play the dominant role. This motivated us to acquire the Auger recombination lifetimes for well-passivated PbS CQDs: we analyzed Cl-passivated 950 nm PbS CQDs (CQD-Cl, Figure 4c) and thin CdS shell 950 nm PbS CQDs (CQD-CdS, Figure 4d). The former had previously been developed as a means of improving passivation

DOI: 10.1021/acsnano.7b06363
ACS Nano XXXX, XXX, XXX–XXX

Table 1. 950 nm PbS Quantum Dot Properties

batch	Auger lifetime (τ_{xx}) (ps)	PLQY in solution (%)	solvent
CQD-OA	17 ± 3	13	toluene
CQD-CdS	35 ± 8	21	toluene
CQD-Cl	38 ± 7	34	toluene
CQD-Per	300 ± 80	*a*	BTA

[a]The perovskite shelling involves a solid-state exchange making PLQY in solution nonapplicable.

Table 2. 1300 nm PbS Quantum Dot Properties

batch	Auger lifetime (τ_{xx}) (ps)	PLQY in solution (%)	solvent
CQD-OLA	113 ± 15	<1	toluene
CQD-CdS	126 ± 10	18	toluene
CQD-Per	250 ± 40	*a*	BTA

[a]The perovskite shelling involves a solid-state exchange making PLQY in solution nonapplicable.

in chalcogenide CQDs.[39] The latter represents one of a small number of strategies to grow shells on lead chalcogenide CQDs; previous studies have found that thin CdS shells have led to improved PLQY evidencing improved passivation.[23]

The Auger lifetime data are summarized in Figure 5a and Table 1. Interestingly, CQD-Cl and CQD-CdS exhibit only moderate improvements compared to CQD-OA. The slight improvement can be attributed to the elimination of surface traps and consequently trap-assisted Auger (Figure 1c) *via* such passivation schemes. However, passivation does not affect intradot Auger recombination in these systems: intradot Auger recombination can be suppressed only by means of band engineering to manipulate wave functions that reduce the matrix element representing the Auger recombination process. The delocalization of wave functions caused by the band diagram in CQD-Per leads to a much more notable enhancement in Auger lifetime, consistent with the theoretical modeling.

Given the motivation to develop PbS CQDs for a wide range of NIR applications, we sought to investigate whether Auger recombination could also improve for larger CQDs with narrower bandgaps. To this end, we investigated the Auger lifetime in 1300 nm PbS CQDs (Figure 5b, Table S8, and Table 2). In this case, untreated PbS CQDs are passivated by oleylamine (CQD-OLA). It is clear that the Auger lifetime has improved for this system as well, albeit to a lesser degree. The reduced enhancement may be attributed to weaker Coulombic interactions between charge carriers in larger CQDs (*i.e.*, large CQDs inherently exhibit slower Auger recombination rates). This is verified theoretically using the model presented earlier. Figure S6 depicts the effect of the core−shell band-edge offset on the Auger rate (as was done for Figure 2c) for two different sizes of PbS CQDs. It is evident that smaller QDs exhibit a more drastic enhancement due to an appropriate shell compared to the unshelled Auger rate value ($E_{CS} - E_{CC}/E_g \rightarrow \infty$).

CONCLUSIONS

In summary, we found that $MAPbI_3$ perovskite shelling decreases the rate of Auger recombination by over 1 order of magnitude in PbS CQD films. Ultrafast TAS allowed the identification and isolation of three different types of Auger recombination: intradot Auger, trap-assisted Auger, and diffusion-assisted Auger. By comparing perovskite shelling to various methods of PbS CQD passivation, we separated the effects of passivation and modal delocalization due to band structure on Auger recombination. Furthermore, theoretical calculations corroborate our findings that only modal delocalization, and not passivation, has a substantial impact on intradot Auger recombination. We posit that the enhanced Auger lifetimes enabled by perovskite shelling could make use of the inherently high mobility of perovskite semiconductors to allow the development of solution-processed electrically injected NIR CW lasing. These results provide the foundation for further work on lead chalcogenides in the pursuit of NIR CW lasing.

EXPERIMENTAL METHODS

Synthesis of Oleic Acid Capped Lead Sulfide (All ~950 nm Dots, ~ 1300 nm CQD-CdS Dot Cores). Quantums dots were synthesized according to the literature.[40] The lead oleate precursor was made by heating PbO in the mix of oleic acid and 1-octadecene at concentrations 0.05 ± 0.2 M under Ar at 100 °C for 16 h. The sulfur precursor was prepared in the glovebox by mixing 420 μL of hexamethyldisilathiane with 10 mL of prepumped ODE.

Synthesis of Oleylamine-Capped Lead Sulfide (~1300 nm CQDs and CQD−PVK Cores). Quantum dots were synthesized according to the literature.[10] However, final PbS dots capped with oleylamine were not stable and over time resulted in aggregation and $PbCl_2$ precipitation. To overcome this issue, we slightly modified the synthesis. A mix of octylamine and hexylamine was introduced before

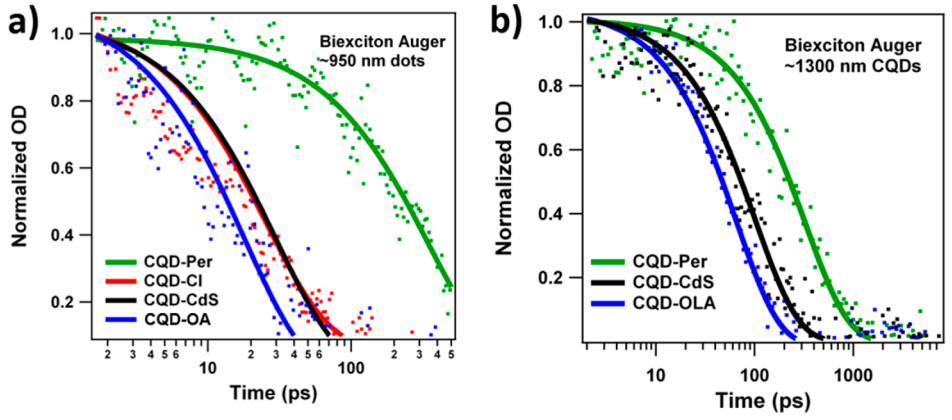

Figure 5. Auger recombination comparison. (a) Intradot biexciton Auger lifetime for 950 nm CQDs. (b) Intradot biexciton Auger lifetime for 1300 nm CQDs.

DOI: 10.1021/acsnano.7b06363
ACS Nano XXXX, XXX, XXX−XXX

quenching with hexane. Based on our observations, short carbon chain amines serve as extra capping ligands and prevent dot aggregation.

Chloride Passivation. Chloride treatment was performed in synthesis during the cooling stage. Tetrabutylammonium chloride (TBAC) was prepared by heating at 200 °C in oleylamine followed by 1 h of pumping at 100 °C. TBAC (0.6 mM) was injected into crude solution at 100 °C during the cooling stage. The reaction mixture was cooled to 35 °C, and the dots were isolated *via* precipitation with acetone and redispersion in toluene.

CdS Passivation. PbS cores were passivated according previously reported protocols.[23]

Perovskite Shell Growth. The perovskite shell was grown on 950 nm CQDs according to literature.[28] The perovskite shell was grown on 1300 nm CQDs with some modifications to the literature. CQD cores (1300 nm) with oleylamine-capped ligands were found to undergo ligand exchange much more readily than 1300 nm CQDs cores with oleic acid capped ligands. In the redispersion step, pure butylamine did not redisperse the CQD−PVK. We mixed some of the initial perovskite precursor solution (in DMF) with butylamine (~1:20) to solubilize the CQD−PVK. We also found that redispersing the CQD−PVK with hexylamine and butanone[41] worked as well.

Steady-State Characterization. Films were measured for linear absorption with a PerkinElmer Lambda 950 UV/vis/NIR spectrophotometer. Photoluminescence quantum yield measurements were collected with an integrating sphere using a Horiba Fluorolog TCSPC system with an iHR monochromator and either a H10330-45 or H10330-75 photomultiplier tube.

Transient Absorption Spectroscopy. A Yb:KGW regenerative amplifier (Pharos, Light Conversion) was used to generate the 1030 nm fundamental (5 kHz). A portion of the beam was sent through an optical parametric amplifier (Orpheus, Light Conversion) to generate the pump pulse. For ~950 nm and ~1300 nm dots, we chose 800 and 1030 nm pumps, respectively; this was done to keep excitations a fixed energy above the bandgaps. The pump and residual fundamental were then sent into an optical bench (Helios, Ultrafast). The fundamental was passed through an optical delay stage to control the time delay between pulses. The fundamental was then focused through a NIR crystal (Ultrafast) to generate an NIR white light continuum probe. The frequency of the pump was halved with an optical chopper. Both the pump and probe were then focused onto the sample, which was translated 1 mm/s. The probe was then directed toward a fiber, which was coupled into a NIR detector (Ultrafast).

ASSOCIATED CONTENT

Supporting Information

The Supporting Information is available free of charge on the ACS Publications website at DOI: 10.1021/acsnano.7b06363.

Theoretical modeling; additional figures and tables (PDF)

AUTHOR INFORMATION

Corresponding Authors

*E-mail: o.voznyy@utoronto.ca.

*E-mail: ted.sargent@utoronto.ca.

ORCID

Rafael Quintero-Bermudez: 0000-0002-4233-395X

Oleksandr Voznyy: 0000-0002-8656-5074

Author Contributions

†R.Q.-B. and R.P.S. contributed equally.

Notes

The authors declare no competing financial interest.

ACKNOWLEDGMENTS

This publication is based in part on work supported by the Ontario Research Fund−Research Excellent Program and by the Natural Sciences and Engineering Research Council (NSERC) of Canada, in particular NSERC Strategic Partnership grant no. 478954-15. We thank Sjoerd Hoogland, Larissa Levina, Elenita Palmiano, Mengxia Liu, and James Fan for their assistance and insightful discussions.

REFERENCES

(1) Protesescu, L.; Yakunin, S.; Bodnarchuk, M. I.; Krieg, F.; Caputo, R.; Hendon, C. H.; Yang, R. X.; Walsh, A.; Kovalenko, M. V. Nanocrystals of Cesium Lead Halide Perovskites (CsPbX3, X = Cl, Br, and I): Novel Optoelectronic Materials Showing Bright Emission with Wide Color Gamut. *Nano Lett.* **2015**, *15*, 3692−3696.

(2) Makarov, N. S.; Guo, S.; Isaienko, O.; Liu, W.; Robel, I.; Klimov, V. I. Spectral and Dynamical Properties of Single Excitons, Biexcitons, and Trions in Cesium-Lead-Halide Perovskite Quantum Dots. *Nano Lett.* **2016**, *16*, 2349−2362.

(3) Mooney, J.; Krause, M. M.; Saari, J. I.; Kambhampati, P. Challenge to the Deep-Trap Model of the Surface in Semiconductor Nanocrystals. *Phys. Rev. B: Condens. Matter Mater. Phys.* **2013**, *87*, 1−5.

(4) Liu, M.; Voznyy, O.; Sabatini, R.; García de Arquer, F. P.; Munir, R.; Balawi, A. H.; Lan, X.; Fan, F.; Walters, G.; Kirmani, A. R.; Hoogland, S.; Laquai, F.; Amassian, A.; Sargent, E. H. Hybrid Organic−inorganic Inks Flatten the Energy Landscape in Colloidal Quantum Dot Solids. *Nat. Mater.* **2016**, *16*, 258−263.

(5) Fan, F.; Voznyy, O.; Sabatini, R. P.; Bicanic, K. T.; Adachi, M. M.; McBride, J. R.; Reid, K. R.; Park, Y.-S.; Li, X.; Jain, A.; Quintero-Bermudez, R.; Saravanapavanantham, M.; Liu, M.; Korkusinski, M.; Hawrylak, P.; Klimov, V. I.; Rosenthal, S. J.; Hoogland, S.; Sargent, E. H. Continuous-Wave Lasing in Colloidal Quantum Dot Solids Enabled by Facet-Selective Epitaxy. *Nature* **2017**, *544*, 75−79.

(6) Shirasaki, Y.; Supran, G. J.; Bawendi, M. G.; Bulović, V. Emergence of Colloidal Quantum-Dot Light-Emitting Technologies. *Nat. Photonics* **2013**, *7*, 13−23.

(7) Yuan, M.; Liu, M.; Sargent, E. H. Colloidal Quantum Dot Solids for Solution-Processed Solar Cells. *Nat. Energy* **2016**, *1*, 16016.

(8) Lita, A. E.; Miller, A. J.; Nam, S. W. Counting near-Infrared Single-Photons with 95% Efficiency. *Opt. Express* **2008**, *16*, 3032−3040.

(9) Michalet, X.; Gambhir, S. S.; Weiss, S. Quantum Dots for Live Cells. *Science (Washington, DC, U. S.)* **2005**, *307*, 538−544.

(10) Cademartiri, L.; Bertolotti, J.; Sapienza, R.; Wiersma, D. S.; Von Freymann, G.; Ozin, G. A. Multigram Scale, Solventless, and Diffusion-Controlled Route to Highly Monodisperse PbS Nanocrystals. *J. Phys. Chem. B* **2006**, *110*, 671−673.

(11) Moreels, I.; Justo, Y.; De Geyter, B.; Haustraete, K.; Martins, J. C.; Hens, Z. Size-Tunable, Bright, and Stable PbS Quantum Dots: A Surface Chemistry Study. *ACS Nano* **2011**, *5*, 2004−2012.

(12) Zhang, J.; Crisp, R. W.; Gao, J.; Kroupa, D. M.; Beard, M. C.; Luther, J. M. Synthetic Conditions for High-Accuracy Size Control of PbS Quantum Dots. *J. Phys. Chem. Lett.* **2015**, *6*, 1830−1833.

(13) Schaller, R. D.; Petruska, M. a; Klimov, V. I. Tunable near-Infrared Optical Gain and Amplified Spontaneous Emission Using PbSe Nanocrystals. *J. Phys. Chem. B* **2003**, *107*, 13765−13768.

(14) Klimov, V. I.; Mikhailovsky, A. A.; Xu, S.; Malko, A.; Hollingsworth, J. A.; Leatherdale, C. A.; Eisler, H.-J.; Bawendi, M. G. Optical Gain and Stimulated Emission in Nanocrystal Quantum Dots. *Science (80-.)* **2000**, *290*, 314−317.

(15) Sukhovatkin, V.; Musikhin, S. Room-Temperature Amplified Spontaneous Emission at 1300 Nm in Solution-Processed PbS Quantum-Dot Films. *Opt. Lett.* **2005**, *30*, 171−173.

(16) Hoogland, S.; Sukhovatkin, V.; Howard, I.; Cauchi, S.; Levina, L.; Sargent, E. H. A Solution-Processed 1.53 Mum Quantum Dot Laser with Temperature-Invariant Emission Wavelength. *Opt. Express* **2006**, *14*, 3273−3281.

(17) Metzger, W. K.; Wanlass, M. W.; Ellingson, R. J.; Ahrenkiel, R. K.; Carapella, J. J. Auger Recombination in Low-Band-Gap N-Type InGaAs. *Appl. Phys. Lett.* **2001**, *79*, 3272−3274.

DOI: 10.1021/acsnano.7b06363
ACS Nano XXXX, XXX, XXX−XXX

(18) Jain, A.; Voznyy, O.; Korkusinski, M.; Hawrylak, P.; Sargent, E. H. Ultrafast Carrier Trapping in Thick-Shell Colloidal Quantum Dots. *J. Phys. Chem. Lett.* **2017**, *8*, 3179−3184.
(19) Gao, Y.; Sandeep, C. S.; Schins, J. M.; Houtepen, A. J.; Siebbeles, L. D. Disorder Strongly Enhances Auger Recombination in Conductive Quantum-Dot Solids. *Nat. Commun.* **2013**, *4*, 2329.
(20) Gao, Y.; Talgorn, E.; Aerts, M.; Trinh, M. T.; Schins, J. M.; Houtepen, A. J.; Siebbeles, L. D. A. Enhanced Hot-Carrier Cooling and Ultrafast Spectral Diffusion in Strongly Coupled PbSe Quantum-Dot Solids. *Nano Lett.* **2011**, *11*, 5471−5476.
(21) Nishihara, T.; Tahara, H.; Okano, M.; Ono, M.; Kanemitsu, Y. Fast Dissociation and Reduced Auger Recombination of Multiple Excitons in Closely Packed PbS Nanocrystal Thin Films. *J. Phys. Chem. Lett.* **2015**, *6*, 1327−1332.
(22) Lin, W.; Fritz, K.; Guerin, G.; Bardajee, G. R.; Hinds, S.; Sukhovatkin, V.; Sargent, E. H.; Scholes, G. D.; Winnik, M. A. Highly Luminescent Lead Sulfide Nanocrystals in Organic Solvents and Water through Ligand Exchange with Poly (Acrylic Acid). *Langmuir* **2008**, *24*, 8215−8219.
(23) Kovalenko, M. V.; Schaller, R. D.; Jarzab, D.; Loi, M. A.; Talapin, D. V. Inorganically Functionalized PbS-CdS Colloidal Nanocrystals: Integration into Amorphous Chalcogenide Glass and Luminescent Properties. *J. Am. Chem. Soc.* **2012**, *134*, 2457−2460.
(24) Konstantatos, G.; Howard, I.; Fischer, A.; Hoogland, S.; Clifford, J.; Klem, E.; Levina, L.; Sargent, E. H. Ultrasensitive Solution-Cast Quantum Dot Photodetectors. *Nature* **2006**, *442*, 180−183.
(25) García-Santamaría, F.; Brovelli, S.; Viswanatha, R.; Hollingsworth, J. A.; Htoon, H.; Crooker, S. A.; Klimov, V. I. Breakdown of Volume Scaling in Auger Recombination in CdSe/CdS Heteronanocrystals: The Role of the Core-Shell Interface. *Nano Lett.* **2011**, *11*, 687−693.
(26) Lim, J.; Jeong, B. G.; Park, M.; Kim, J. K.; Pietryga, J. M.; Park, Y. S.; Klimov, V. I.; Lee, C.; Lee, D. C.; Bae, W. K. Influence of Shell Thickness on the Performance of Light-Emitting Devices Based on CdSe/Zn 1- X Cd X S Core/shell Heterostructured Quantum Dots. *Adv. Mater.* **2014**, *26*, 8034−8040.
(27) Cao, Y. W.; Banin, U. Growth and Properties of Semiconductor Core/Shell Nanocrystals with InAs Cores. *J. Am. Chem. Soc.* **2000**, *122*, 9692−9702.
(28) Yang, Z.; Janmohamed, A.; Lan, X.; García De Arquer, F. P.; Voznyy, O.; Yassitepe, E.; Kim, G. H.; Ning, Z.; Gong, X.; Comin, R.; Sargent, E. H. Colloidal Quantum Dot Photovoltaics Enhanced by Perovskite Shelling. *Nano Lett.* **2015**, *15*, 7539−7543.
(29) Sytnyk, M.; Yakunin, S.; Schöfberger, W.; Lechner, R. T.; Burian, M.; Ludescher, L.; Killilea, N. A.; YousefiAmin, A.; Kriegner, D.; Stangl, Δ. J.; Groiss, H.; Heiss, W. Quasi-Epitaxial Metal-Halide Perovskite Ligand Shells on PbS Nanocrystals. *ACS Nano* **2017**, *11*, 1246−1256.
(30) Ngo, T. T.; Suarez, I.; Sanchez, R. S.; Martinez-Pastor, J. P.; Mora-Sero, I. Single Step Deposition of an Interacting Layer of a Perovskite Matrix with Embedded Quantum Dots. *Nanoscale* **2016**, *8*, 14379−14383.
(31) García de Arquer, F. P.; Gong, X.; Sabatini, R. P.; Liu, M.; Kim, G.-H.; Sutherland, B. R.; Voznyy, O.; Xu, J.; Pang, Y.; Hoogland, S.; Sinton, D.; Sargent, E. Field-Emission from Quantum-Dot-in-Perovskite Solids. *Nat. Commun.* **2017**, *8*, 14757.
(32) Gong, X.; Yang, Z.; Walters, G.; Comin, R.; Ning, Z.; Beauregard, E.; Adinolfi, V.; Voznyy, O.; Sargent, E. H. Highly Efficient Quantum Dot near-Infrared Light-Emitting Diodes. *Nat. Photonics* **2016**, *10*, 253−257.
(33) Cragg, G. E.; Efros, A. L. Suppression of Auger Processes in Confined Structures. *Nano Lett.* **2010**, *10*, 313−317.
(34) Climente, J. I.; Movilla, J. L.; Planelles, J. Auger Recombination Suppression in Nanocrystals with Asymmetric Electron-Hole Confinement. *Small* **2012**, *8*, 754−759.
(35) Ning, Z.; Gong, X.; Comin, R.; Walters, G.; Fan, F.; Voznyy, O.; Yassitepe, E.; Buin, A.; Hoogland, S.; Sargent, E. H. Quantum-Dot-in-Perovskite Solids. *Nature* **2015**, *523*, 324−328.
(36) Castaneda, J. A.; Nagamine, G.; Yassitepe, E.; Bonato, L. G.; Voznyy, O.; Hoogland, S.; Nogueira, A. F.; Sargent, E. H.; Cruz, C. H. B.; Padilha, L. A. Efficient Biexciton Interaction in Perovskite Quantum Dots under Weak and Strong Confinement. *ACS Nano* **2016**, *10*, 8603−8609.
(37) Stewart, J. T.; Padilha, L. A.; Qazilbash, M. M.; Pietryga, J. M.; Midgett, A. G.; Luther, J. M.; Beard, M. C.; Nozik, A. J.; Klimov, V. I. Comparison of Carrier Multiplication Yields in PbS and PbSe Nanocrystals: The Role of Competing Energy-Loss Processes. *Nano Lett.* **2012**, *12*, 622−628.
(38) Nootz, G.; Padilha, L. A.; Levina, L.; Sukhovatkin, V.; Webster, S.; Brzozowski, L.; Sargent, E. H.; Hagan, D. J.; Van Stryland, E. W. Size Dependence of Carrier Dynamics and Carrier Multiplication in PbS Quantum Dots. *Phys. Rev. B: Condens. Matter Mater. Phys.* **2011**, *83*, 1−7.
(39) Thon, S. M.; Ip, A. H.; Voznyy, O.; Levina, L.; Kemp, K. W.; Carey, G. H.; Masala, S.; Sargent, E. H. Role of Bond Adaptability in the Passivation of Colloidal Quantum Dot Solids. *ACS Nano* **2013**, *7*, 7680−7688.
(40) Hines, M. A.; Scholes, G. D. Colloidal PbS Nanocrystals with Size-Tunable Near-Infrared Emission: Observation of Post-Synthesis Self-Narrowing of the Particle Size Distribution. *Adv. Mater.* **2003**, *15*, 1844−1849.
(41) Kiani, A.; Sutherland, B. R.; Kim, Y.; Ouellette, O.; Levina, L.; Walters, G.; Dinh, C. T.; Liu, M.; Voznyy, O.; Lan, X.; Labelle, A. J.; Ip, A. H.; Proppe, A.; Ahmed, G. H.; Mohammed, O. F.; Hoogland, S.; Sargent, E. H. Single-Step Colloidal Quantum Dot Films for Infrared Solar Harvesting. *Appl. Phys. Lett.* **2016**, *109*.18310510.1063/1.4966217

DOI: 10.1021/acsnano.7b06363
ACS Nano XXXX, XXX, XXX−XXX